Numerical Simulation and Comparison with Experiment for Self-Excited Oscillations in a Diffuser Flow

T. Hsieh*
Naval Surface Weapons Center, Silver Spring, Maryland
T. J. Bogar†
McDonnell Douglas Research Laboratories, St. Louis, Missouri
and
T. J. Coakley‡
NASA Ames Research Center, Moffett Field, California

This paper describes numerical simulations of self-excited oscillations in a two-dimensional transonic diffuser flow obtained by solving the Navier-Stokes equations with a two-equation turbulence model. Comparisons were made between the computational results and experimental data. For the mean flowfields, agreement between computation and experiment is good for the wall pressures, shock location, and separation and reattachment points. However, the thickness of the computed recirculation zone is about 50% of the measured thickness. For the fluctuating flowfields, a great deal of qualitative similarity exists between computation and experiment; however, the predicted oscillation frequency is about 50% higher than the measured value. The formation of a succession of downstream-traveling counter-rotating vortices, as seen experimentally, is also vividly displayed in the numerical results.

Nomenclature

E = specific total energy
f = frequency
H = throat height
k = turbulent kinetic energy
N = time-step count
p,p' = instantaneous and fluctuating pressure
p_e = exit pressure
p_r = ratio of p_e to p_t
p_t = total pressure
t = time
u,u' = instantaneous and fluctuating streamwise velocity
v,v' = instantaneous and fluctuating vertical velocity
x,y = streamwise and vertical coordinates, $x=0$ at throat, $y=0$ at bottom wall
μ = viscosity
ρ = density
σ = shock
ϕ = phase, with respect to shock phase
ω = specific dissipation rate of turbulent kinetic energy

Introduction

RECENT test of ramjet propulsion systems have revealed undesirable, high-amplitude pressure fluctuations caused by instability in the ramjet combustor.[1] The most troublesome oscillations are in the frequency range 100 – 500 Hz, and the corresponding rms amplitudes of pressure fluctuation can reach up to 20% of the mean pressure in the combustor. The interaction between the inlet and the combustor flowfields is one of the major causes of instability for the entire system. Because of the complicated chemical reactions and thermal additions in the combustor, a numerical simulation of the entire system is currently beyond reach. However, it is possible to simulate numerically the unsteady inlet flowfields separately as a first step to a better understanding of inlet/combustor-coupling-induced instabilities.

Successful numerical simulations of unsteady flow in inlets obtained by solving the two-dimensional, time-dependent, compressible, Reynolds-averaged, thin-layer Navier-Stokes equations with a two-equation turbulence model have been reported.[2-7] In Ref. 2, when an attempt was made to compute a steady-state solution for the diffuser configuration shown in Fig. 1 at $p_r=0.72$ using a time asymptotic approach, the terminal shock continued to oscillate with time, not achieving a steady state. This is a strong indication of a self-excited oscillating flow. Although numerical simulations of self-excited oscillations in diffuser flows were reported in Ref. 7, the computation was for a configuration for which no detailed experimental information about the fluctuating flowfields was given.

Extensive experimental data do exist for the unsteady flowfield for the diffuser configuration shown in Fig. 1, [8-12] in particular for the case $p_r=0.72$, which exhibits the self-excited oscillations. Therefore, careful computations have been performed for this case, focusing on the unsteady aspects of the flow, so that a thorough comparison of the numerical results against the experimental data can be performed. The goals are twofold: 1) to test and improve the capability of the present numerical code in simulating a complicated unsteady flowfield, and 2) to understand the physics of a flow of practical importance.

Numerical Procedures

The numerical procedures used for solving the Navier-Stokes equations for the geometry shown in Fig. 1 are described in Refs. 2 and 7. A brief outline is given in this section.

The basic equations are the two-dimensional, compressible, time-dependent, Reynolds-averaged, thin-layer Navier-Stokes equations for the conservation of mass, momentum, and energy, together with the two-equation turbulence model of Wilcox and Rubesin[13] for the turbulence kinetic energy

Presented as Paper 85-1475 at the AIAA/SAE/ASME/ASEE 21st Joint Propulsion Conference, Monterey, CA, July 8-10, 1985; received Feb. 11, 1986; revision received Oct. 15, 1986.

*Research Engineer. Associate Fellow AIAA.
†Scientist. Senior Member AIAA.
‡Research Scientist. Member AIAA.

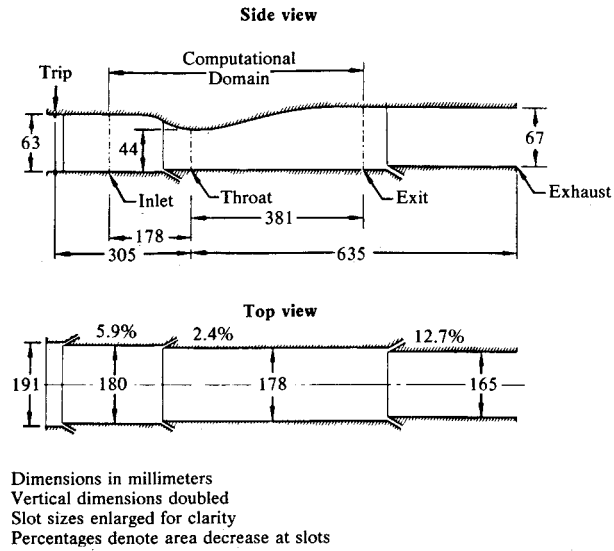

Fig. 1 Diffuser configuration.

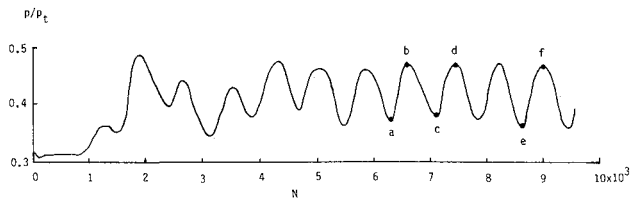

Fig. 2 Time history of local pressure variation on top wall at $x/H=2.179$.

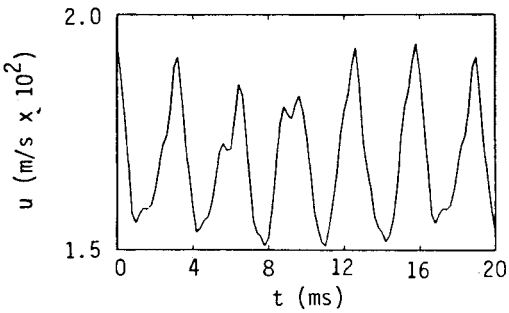

a) Waveform.

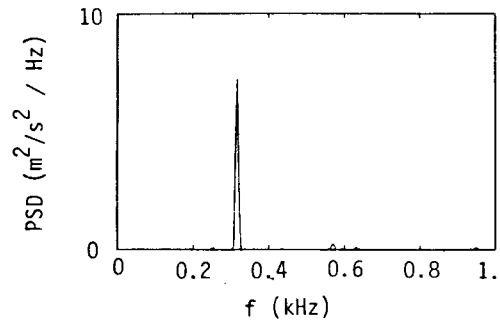

b) Power spectral density.

Fig. 3 Computed μ-velocity wave form and PSD distribution at $x/H=8.369$ and $y/H=1.012$.

and specific dissipation rate of kinetic energy. (The constants used in the turbulence model can be found in Ref. 7.) In addition, the equation of state for a perfect gas is assumed. There are therefore seven equations for the seven variables ρ, u, v, E, p, k, and ω. All equations are written in conservation form. A modified MacCormack's hybrid method[14] is used to solve the basic equations.

The inflow and outflow boundaries are located at $x/H=-4.04$, (-178 mm) and $x/H=8.66$ (381 mm) denoted as the inlet and exit stations in Fig. 1. In the core-flow region of the inflow boundary, the total pressure and temperature were set at 135 kPa and 292 K, respectively. The vertical velocity is set to zero, and the streamwise velocity and static pressure are obtained by solving the steady-flow energy equation and the characteristic relations, assuming a locally one-dimensional flow. This produced a Reynolds number at the inflow boundary, based on inflow inlet height, of 8.22×10^5. The boundary-layer thicknesses on the top and bottom walls at the inflow plane are prescribed according to experimentally obtained values[10] (9% of H on the top wall and 4.5% of H on the bottom).

At the outflow boundary, the static pressure is prescribed. The streamwise velocity is obtained by extrapolation of the locally one-dimensional characteristic relations. Zero-gradient conditions are used for the entropy, the vertical velocity, and the turbulence variables.

On the top and bottom walls, the no-slip and adiabatic wall conditions are imposed. The wall pressures are computed as an integral part of MacCormack's hybrid algorithm. The turbulent kinetic energy is set to zero, and an analytic formula for ω ($\omega=133\mu/\rho y^2$) is used for a few points near the wall. (Note that ω is not defined at the wall.)

The initial flowfield was prescribed using the one-dimensional, steady duct solution. Near the top and bottom wall, velocity components were modified using the one-seventh power law with a linear laminar-sublayer profile for u and the wall slope for v. Appropriate initial profiles for k and ω^2 were also implemented.

All calculations were carried out on a mesh, with 80 points in the streamwise direction and 50 points in the vertical direction. The mesh was exponentially stretched in the vertical direction near the top and bottom walls in a manner that assumed the presence of at least two points in the laminar sublayer. The streamwise mesh points were clustered in the region between $x/H=1$ and 3 with constant spacing of $H/15$, in order to improve resolution of the terminal shock.

The computation method proved to be robust in providing solutions to various sets of boundary conditions given in Refs. 4–6. The present calculations were performed on the NASA-ARC CRAY-X-MP computer and used 3.6×10^{-4} CPU-s/mesh-point/time step. Each time step corresponded to a 4×10^{-6}-s interval for the physical flow.

During the calculations, data for the entire flowfield were saved at every 50 time steps. Figure 2 shows the time history of the top-wall static pressure at $x/H=2.179$ throughout the computation. After a transient period of about 3000 time steps, the self-excited nature of the flow is quite evident as the pressure fluctuation settles into a highly periodic oscillation as the computation proceeds. Flowfield data (p, u, and v) from the last five cycles ($N=5300-N=9300$) were used for detailed analysis and comparison with experimental results.

The highly periodic nature of the computed flow persists through the flowfield and includes all flow variables. Figure 3a shows the streamwise velocity fluctuation waveform near the downstream boundary. The power-spectral-density distribution (PSD, Fig. 3b) of the waveform shows a single large peak at 317 Hz; departures from strict periodicity appear as relatively insignificant bumps on the PSD.

Experimental Arrangement

The experimental arrangement, data acquisition and reduction procedures, and experimental results are discussed in detail in Ref. 12.

The diffuser model (Fig. 1) is a converging/diverging channel with an exit-to-throat area ratio of 1.52. The aspect ratio at the throat is 4.05. The top-wall boundary layer is tripped ahead of the converging channel section. Reference 10 presents details of the experimental facility and, together

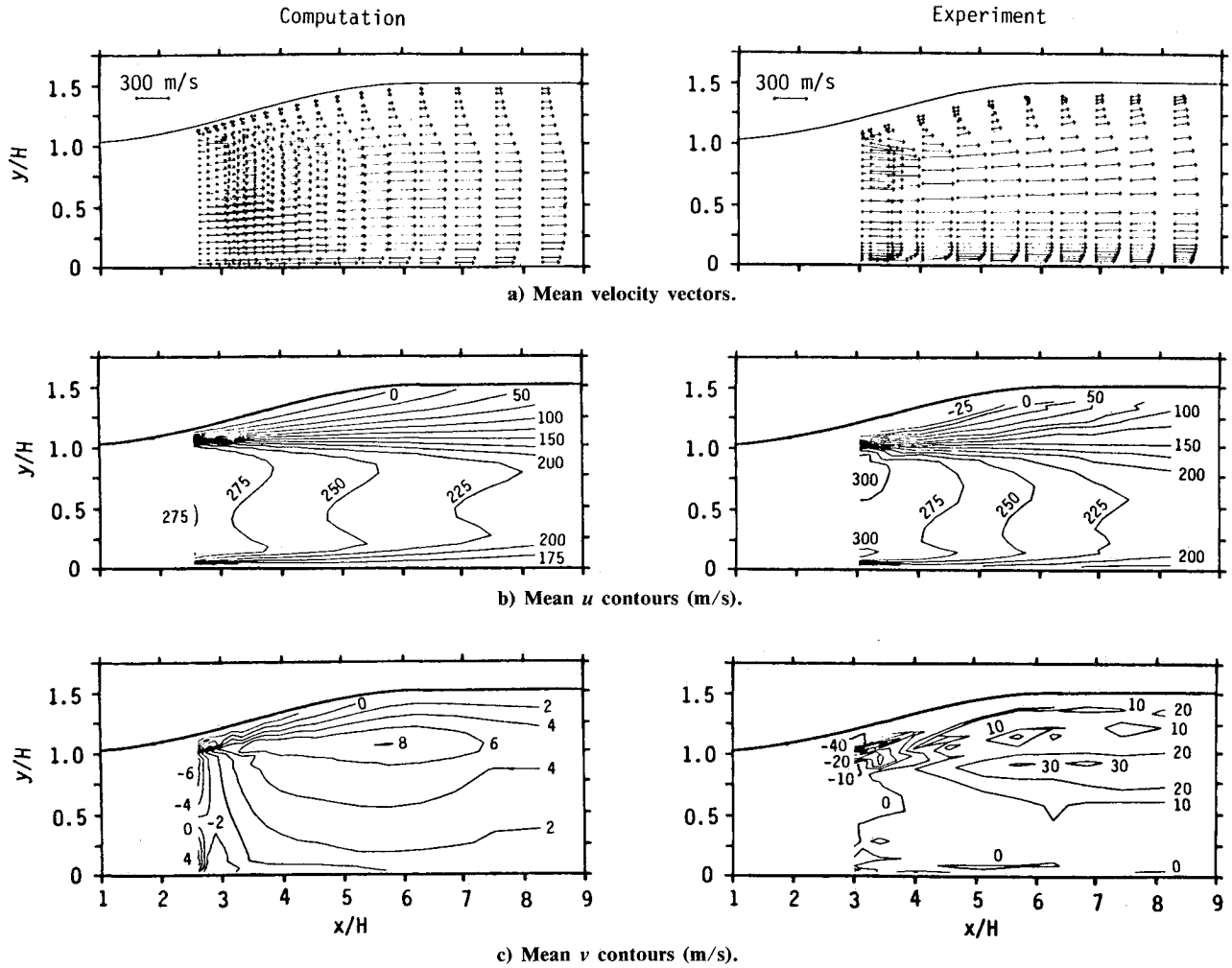

a) Mean velocity vectors.

b) Mean u contours (m/s).

c) Mean v contours (m/s).

Fig. 4 Comparisons of mean velocity vectors, u and v velocity contours.

with Ref. 9, describes the unexcited flowfield for this model in terms of shock location, wall and core pressures (time-mean and rms fluctuation values), and laser Doppler velocimetry (LDV) measurement of the subsonic flowfield.

At $p_r = 0.72$, the shock was sufficiently strong to cause separation in the top-wall boundary layer. At this operating condition, the flow has a natural oscillation frequency of approximately 210 Hz, as determined from shock location and wall and core flow pressure measurements.[10]

Data Reduction Procedure

The computational results were ensemble-averaged using the same procedure that was applied to the experimental data.[12] However, since no direct shock location signal was available by which the computational results might be sorted, one computational grid point corresponding to a location at the upstream edge of the experimental data range was chosen as a reference point for each of the computed flow quantities investigated (u, v, and p). The ensemble averaging of data from all other grid points was carried out with respect to the reference point. To bring the computational phases into correspondence with the experimental, that is, to reference the computational phases to the shock phase, the phase at the reference point was shifted to be equal to the experimentally obtained phase at the same point. All other computational phases were shifted by the same amount.

Comparison and Discussion

Mean Flowfields

Comparisons between computational and experimental results for wall pressure distributions for the case under investigation may be found in Ref. 4. The agreement is good for wall pressure distribution (within 5%), the location of terminal shock, and thus the point of (shock induced) separation.

Plots of velocity vectors and contours of u and v time-mean flowfield are shown in Fig. 4 for both the computational and experimental results. As shown in the velocity vector plot (Fig. 4a), the point of flow reattachment on the top wall is seen to agree well at $x/H = 6.0$ for both computation and experiment. The reattachment point was determined by the intersection of the zero-streamwise-velocity line and the wall in the experiment and by the vanishing of skin friction along the top wall with positive slope in the computation. The experimental recirculation zone is about twice as thick as the computational result. This difference may be attributed partly to the insufficient number of mesh points in the vertical direction[16] and partly to the three-dimensional effects in the experiment, which tend to thicken the boundary layer in the plane of symmetry where the data were measured (see Ref. 10).

The comparison of u contours (Fig. 4b) show considerable similarity between the experiment and computation. The experiment shows a slightly higher velocity in the core region, probably because of the greater blockage caused by the recirculation zone.

The v contours (Fig. 4c) also show considerable qualitative similarity. Again, the experimental magnitudes are higher because of the greater deflection of the flow around the larger separation zone. The experimental data for v show a moderate amount of scatter both in the mean data and in the fluctuations discussed below. This is because the LDV beams were aligned at $+/-$ 45 deg to the horizontal and because the vertical velocity component was determined from the difference between two large values of nearly equal magnitude.

Terminal Shock Oscillation

The oscillation of the terminal shock as determined by the computation is clearly demonstrated by the time history of the top-wall pressure shown in Fig. 2. The time-dependent shock position may also be obtained by plotting the pressure distribution in the vicinity of the shock at several different time steps after the oscillation is firmly established ($N > 5000$). In Fig. 5, the pressure distribution for the top wall is plotted for six different time steps (denoted by letters a – f in Fig. 2), at which time the pressure in Fig. 2 is at a maximum or a minimum. Figure 5 shows that the amplitudes of the shock oscillation vary between 0.07 and 0.1 throat heights. This result is to be compared with the measured mean amplitude of 0.06 throat heights, again showing reasonably good agreement.

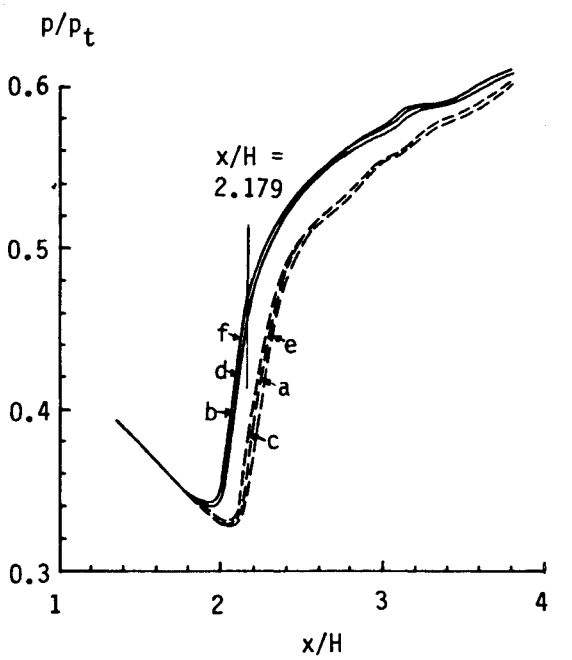

Fig. 5 Top wall pressure distribution near the terminal shock at six different time steps.

Fluctuating Velocity Fields

Before comparison of the fluctuating velocity field, the reader is to be reminded about the difference in frequency of oscillation between computation (317 Hz) and experiment (210 Hz). This difference may be attributed to the difference in the downstream boundary. In computation, the exit plane is located at $x/H = 8.6$, and the local measured pressure of $p/p_t = 0.72$ was used as the exit pressure. In the experiment, the diffuser is extended to $x/H = 14$, with a suction slot located at $x/H = 9.8$. A study of downstream boundary effects is in progress,[17] and preliminary results indicate that the frequency of oscillation reduces as the diffuser length increases. Therefore, the comparison of phase described in this section is entirely qualitative.

The comparison of amplitude and phase distributions for the streamwise velocity fluctuations are shown in Fig. 6. The computed amplitudes (Fig. 6a) are generally higher, particularly at the upstream edge of the recirculation zone; however, both the computation (left column, Fig. 6) and experiment (right column, Fig. 6) show the majority of the activity to be in the shear layer at the edge of the recirculation zone. As the shock oscillates, so does the boundary-layer thickness. Both the measurement and computation represent the Eulerian velocity at a fixed location whose distance from the wall corresponds to some fraction of the boundary-layer thickness. This fraction changes as the boundary-layer thickness oscillates, and the velocity associated with this fraction varies according to the shape of the velocity profile. The steeper the gradient or the greater the thickness variation, the greater the velocity fluctuation. The disparity between the experimental and computed streamwise velocity fluctuation amplitudes is probably the result of differences in the individual boundary-layer characteristics.

The computation and experiment show striking agreement in the phase distribution (Fig. 6b) as well. Two interesting points are noted. First, since the disturbance propagates in a direction perpendicular to the constant-phase contours, both results show a vertical flapping (transverse oscillation) of the core flow, denoted by the horizontal phase contours throughout much of the flow. Immediately downstream of the shock,

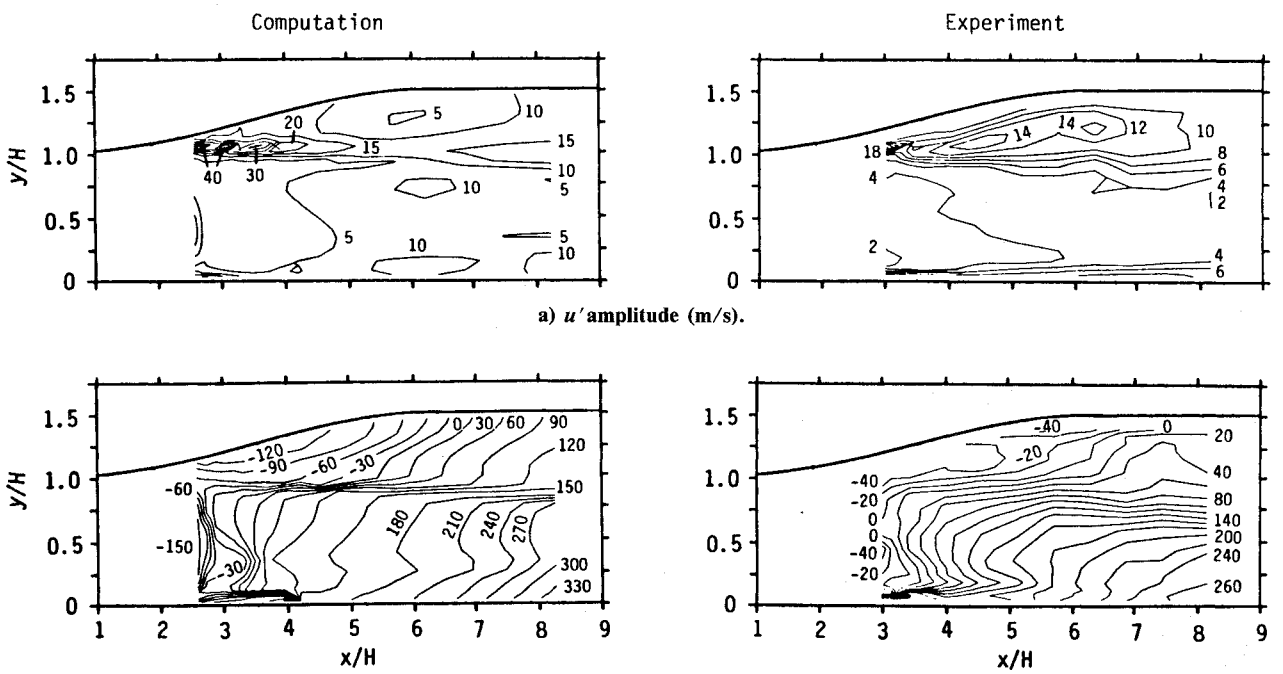

a) u' amplitude (m/s).

b) u' phase (deg).

Fig. 6 Comparisons of amplitude and phase contour for the fluctuating streamwise velocity.

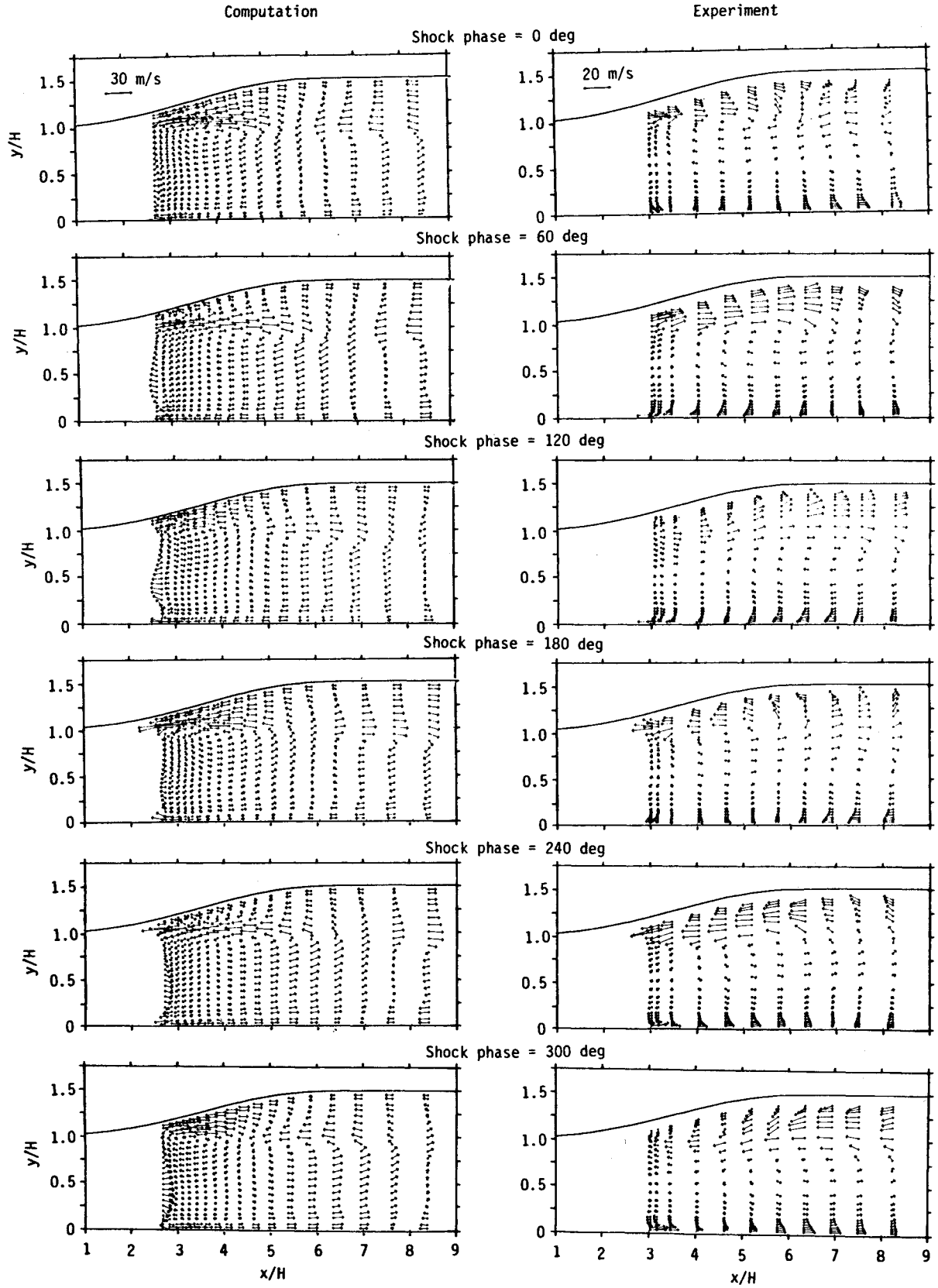

Fig. 7 Temporal development of ensemble-average velocity vector fluctuations.

however, the fluctuation in the core flow is longitudinal (vertical phase contours) for a short distance. Second, the phase that exists immediately after the shock in the core flow appears considerably farther downstream in the top-wall boundary layer in both cases. The longitudinal oscillation is quickly and completely overwhelmed by the boundary-layer-related transverse motion. The boundary layer seems to be a more effective medium for the propagation of the shock-related disturbances than the core flow.

The amplitude of v' is relatively small compared to u'. The amplitudes and phases for v' are not shown here but may be found in Ref. 18. The phase distributions of these quantities for the experiment and computation are quite similar, and both show an essentially streamwise propagation

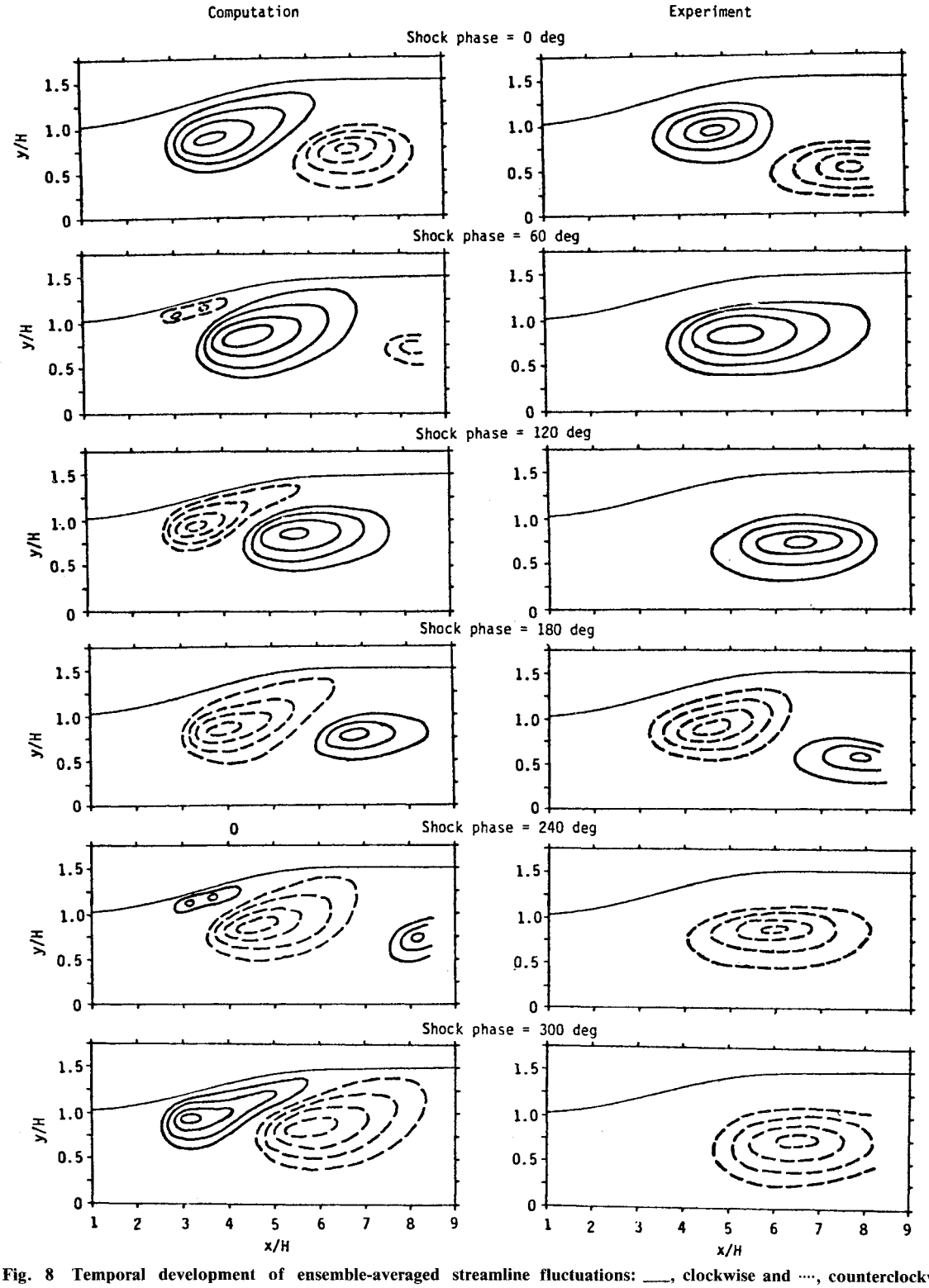

Fig. 8 Temporal development of ensemble-averaged streamline fluctuations: ___, clockwise and ····, counterclockwise.

of the vertical velocity disturbance, as signified by the generally vertical phase contours. This pattern is consistent with the existence of a transverse oscillation (flapping) of the core flow.

The horizontal and vertical velocity fluctuation can be combined to provide a picture of the velocity vector fluctuations as the oscillation proceeds through its cycle. Figure 7 shows the evolution of the experimental and computed vector fields at six equally spaced phases. One striking result of the experimental investigation was the discovery of a succession of counter-rotating structures being convected through the top-wall boundary layer. This feature is also vividly represented in the computational results. In both cases, the structures are seen to originate at the upstream edge of the recirculation zone. Because many more grid points are provided in the computation than measured points in the experiment, the computed results give more detail, particularly in this region.

The structure of the fluctuating velocity fields might better be visualized by sketching the streamlines associated with the rotating structures (Fig. 8). The solid and dotted lines denote clockwise and counterclockwise rotation, respectively.

From the computed results (Fig. 8, left column), three distinct stages of development for each of the rotating structures can be distinguished:

1) The production stage. Several small vortices, rotating in

the same direction, are produced near the upstream edge of the recirculation zone, where the mean velocity gradient is large. The production mechanism appears to occur near a shock phase of 60 deg for the counterclockwise-rotating structures and near 240 deg for the clockwise-rotating structures.

2) The growth stage. The small vortices merge into a large structure, which continues to gain strength as it moves downstream and toward the center of the diffuser.

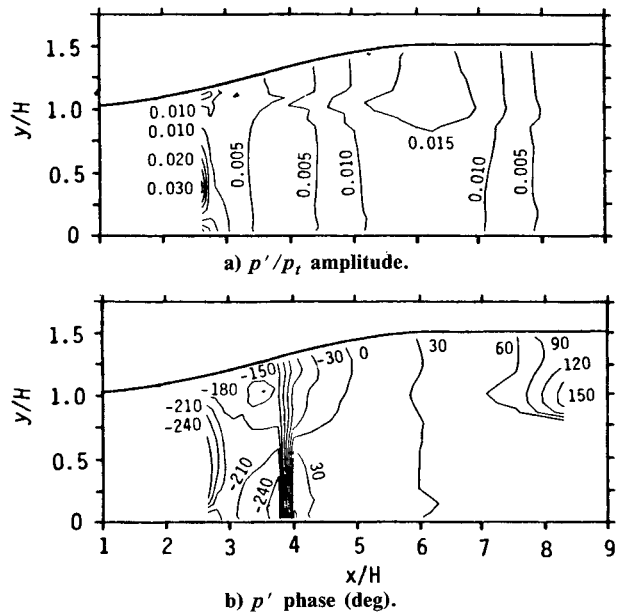

a) p'/p_t amplitude.

b) p' phase (deg).

Fig. 9 Computed pressure fluctuation amplitude and phase contours.

3) The convection stage. The vortex stops growing as it moves past the exit plane and out of both the computation and measurement fields.

Two major differences appear between the computation and experiment as shown in Fig. 8. First, the production and the early growth stages do not appear in the experimental results. This is probably because no measurements were made near the walls owing to practical considerations with the LDV and data acquisition systems. These stages may indeed exist in the experiment, but they were not measured. Second, the length scales associated with the structures are shorter for the computation. The convection speeds for the structures have been estimated to be comparable, 70 m/s for the experiment and 68 m/s for the computation. The difference in length scale results primarily from the oscillation frequency difference between the experiment and computation.

There is no comparable experimental pressure data for the entire flowfield; measurements were made at only a limited number of stations along the top wall and along a line 0.432 throat height above the bottom wall. Figure 10 shows a comparison between the computation and experiment where such a comparison is possible. As was the case with the velocity fluctuations, the computed pressure fluctuations are generally higher amplitude than the experimentally determined amplitudes.

Fluctuating Pressure Fields

Contour plots of computed amplitude and phase for the fluctuating pressure field are shown in Fig. 9. Except for very near the shock, the fluctuation amplitudes remain relatively small, about 1% of the total pressure, throughout the flowfield (Fig. 9a). There are distinct minima at approximately $x/H=4$ and $x/H=8.5$. The first minimum corresponds to a large, concentrated phase shift (Fig. 9b) of approximately 180 deg, indicating a standing-wave-like character to the flow.

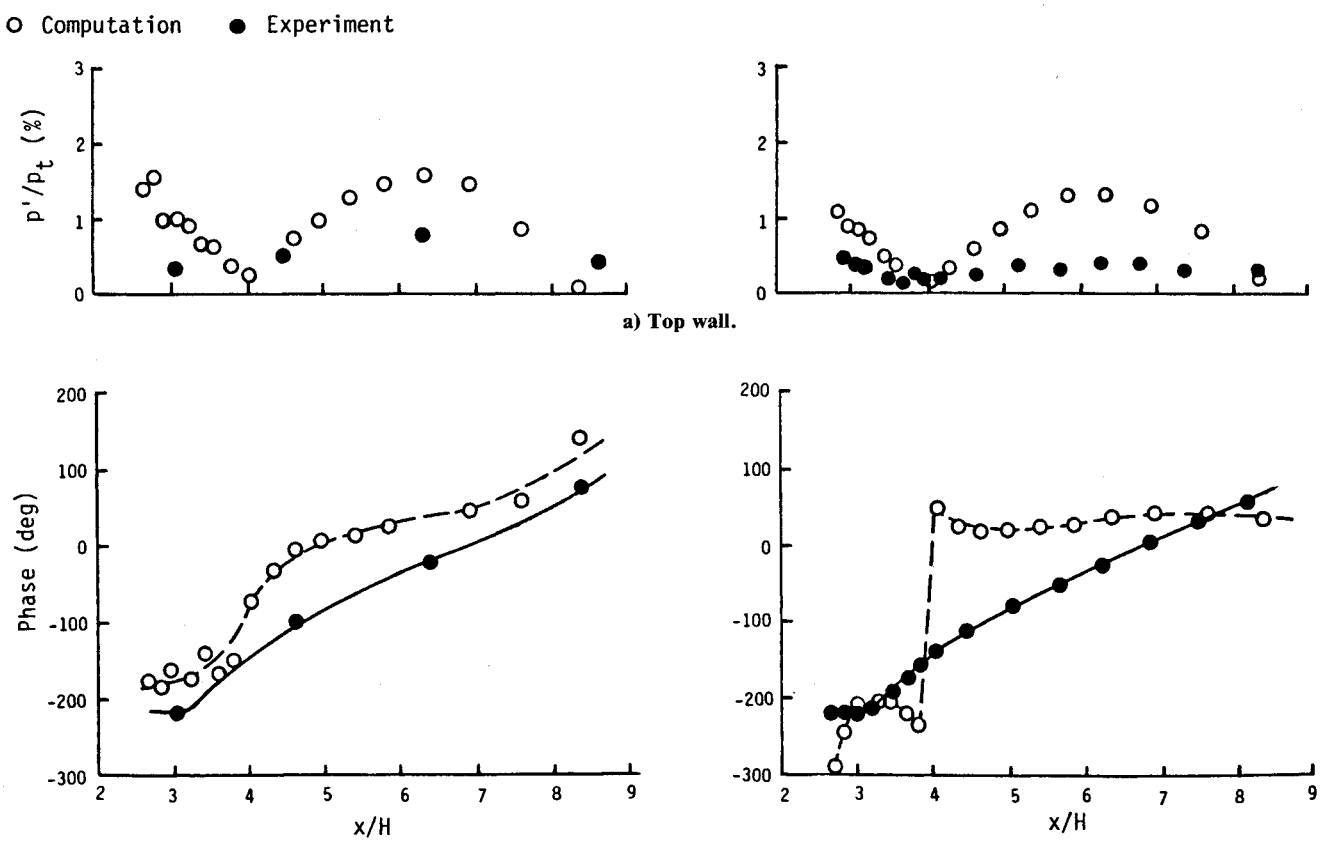

a) Top wall.

b) Core ($y/H=0.432$).

Fig. 10 Comparisons of amplitude and phase of pressure fluctuation.

The minima in the computed amplitudes appear clearly along the top wall and in the core. The experimental data also show a decided minimum in the core flow; however, it is located somewhat farther upstream, at $x/H=3.5$. There are insufficient data to define a minimum from the top-wall experimental results.

Significant differences appear between the experiment and computation in the pressure fluctuation phases. The experimental data for both the wall and core show a smooth, steady increase downstream, indicating the presence of a planar, strictly downstream-convected disturbance. This is compared with the sharp phase shift for the core flow data present in the computation. The phase shift is considerably less pronounced, but still visible, in the computed top-wall pressure data.

Some light may be shed on the origin of the difference between the computation and experiment by considering the possible mechanisms at work in the flow. A model has been developed[15] in which the organized unsteady flow occurring in transonic internal flows results from the interaction of three primary waves: upstream- and downstream-traveling acoustic waves and a downstream-traveling "interface wave." As an upstream-traveling acoustic wave impinges on the shock, it produces a reflected acoustic wave but, in addition, the recoil of the shock causes a disturbance in the separated boundary layer (interface wave), which is convected downstream at approximately half the core flow velocity. Both the computation and experiment support the existence of such a phenomenon (Fig. 7).

The differences between experiment and computation might be attributed to the relative contributions of these three mechanisms to the resultant wave. The interface wave is clearly a purely viscous phenomenon, while acoustic waves are inviscid. The computation shows the core flow pressure disturbance to be dominated by acoustic disturbances, resulting in the standing-wave-like pattern. In the top-wall boundary layer, however, the phase distribution looks more nearly convective, gradually increasing without a sharp phase shift. Since the experimental boundary layer is considerably thicker than the computational one, it is reasonable that the viscous phenomenon would dominate. The displacement thickness changes associated with the boundary-layer fluctuations are sufficiently large to make their presence felt in the interior of the core flow. Hence, both the wall and core data show a convected wave in the experimental data.

Summary

The result of the comparison between experimental data and a numerical simulation of self-excited oscillations in a two-dimensional transonic diffuser obtained by solving the Navier-Stokes equations with a two-equation turbulence model can be summarized as follows:

1) The computed and experimental mean flows show reasonable agreement. The computation predicts the measured separation and reattachment points for the recirculation zone; however, the predicted zone thickness is only half the measured value. The computed boundary layer is also somewhat thinner. Vertical mesh point distribution that is insufficient to resolve the viscous effects and three-dimensional effects in the experiment is the major source of the difference.

2) The computed amplitudes of all the oscillating flow quantities are somewhat higher than the measured values; however, a great deal of qualitative similarity exists for the fluctuating velocity fields. The predicted frequency is about 50% higher than the experimental value. This difference in frequency may be attributed to the difference in downstream boundary between computation and experiment.

3) Both computation and experiment show the vertical flapping of the core flow, resulting from the thickness variations of the top-wall boundary layer. The effects of the shock oscillation appear to propagate faster through the top-wall boundary layer than through the core flow.

4) The formation of a succession of downstream-traveling, counter-rotating vortices, which appear in the experiment, are also vividly revealed in the numerical results.

5) Three possible oscillation mechanisms have been suggested, with the nature of the result fluctuation depending on the relative contributions of the three. Viscous mechanisms seem to dominate the experiment, with the thicker boundary layer, more than the computation.

Acknowledgments

The work of the first author was sponsored by the Office of Naval Research and monitored by Dr. R. E. Whitehead. The work of the second author was supported by the McDonnell Douglas Independent Research and Development Program. The computer time for the computations was provided by NASA Ames Research Center. Helpful discussions with Dr. M. Sajben are gratefully acknowledged.

References

[1]Clark, W. H., "Experimental Investigation of Pressure Oscillations in a Solid Dump Ramjet Combustor," *Journal of Spacecraft*, Vol. 19, Jan.-Feb. 1982, pp. 47-53.

[2]Coakley, T. J. and Bergmann, M. Y., "Effects of Turbulence Model Selection on the Prediction of Complex Aerodynamic Flows," AIAA Paper 79-0070, Jan. 1979.

[3]Liou, M. S., Coakley, T. J., and Bergmann, M. Y., "Numerical Simulation of Transonic Flows in Diffusers," AIAA Paper 81-2140, June 1981.

[4]Hsieh, T., Wardlaw, A. B. Jr., Collins, P. and Coakley, T., "Numerical Investigation of Unsteady Inlet Flow Fields," AIAA Paper 84-0031, Jan. 1984.

[5]Hsieh, T., Wardlaw, A. B. Jr., and Coakley, T., "Numerical Simulation of a Ramjet Inlet Flow in Response to Large Amplitude Combustor Pressure Oscillation," AIAA Paper 84-1363, June 1984.

[6]Hsieh, T. and Wardlaw, A. B. Jr. "Numerical Simulation of Unsteady Flow in a Ramjet Inlet," *Proceedings of the 14th Congress of the International Council of the Aeronautical Science*, Sept. 1984, ICAS-84-1.9.2., 1984.

[7]Liou, M. S. and Coakley, T. J., "Numerical Simulations of Unsteady Transonic Flow in Diffusers," *AIAA Journal*, Vol. 22, Aug. 1984, pp. 1139-1145.

[8]Chen, C. P., Sajben, M., and Kroutil, J. C., "Shock Wave Oscillations in a Transonic Diffuser Flow," *AIAA Journal*, Vol. 17, Oct. 1979, pp. 1076-1083.

[9]Salmon, J. T., Bogar, T. J., and Sajben, M., "Laser Doppler Velocimeter Measurements in Unsteady, Separated Transonic Diffuser Flows," *AIAA Journal*, Vol. 21, Dec. 1983, pp. 1690-1697.

[10]Bogar, T. J., Sajben, M., and Kroutil, J. C. "Characteristic Frequencies of Transonic Diffuser Flow Oscillations," *AIAA Journal*, Vol. 21, Sept. 1983, pp. 1232-1240.

[11]Sajben, M., Bogar, T. J., and Kroutil, J. C., "Forced Oscillation Experiments in Supercritical Diffuser Flows," *AIAA Journal*, Vol. 22, April 1984, pp. 465-474.

[12]Bogar, T. J., "Structure of Self-Excited Oscillations in Transonic Diffuser Flows," *AIAA Journal*, Vol. 24, Jan. 1986, pp. 54-61.

[13]Wilcox, D. C. and Rubesin, M. W., "Progress in Turbulence Modeling for Complex Flow Fields Including Effects of Compressibility," NASA TP-1517, 1980.

[14]MacCormack, R. W., "An Efficient Numerical Method for Soling the Time-Dependent Compressible Navier-Stokes Equations at High Reynolds Number," *Computing in Applied Mechanics*, ASME, Vol. 18, 1976, pp. 49-64.

[15]Sajben, M. and Bogar, T. J., "Unsteady Transonic Flow in a Two-Dimensional Diffuser: Interpretation of Test Results," AFOSR-TR-83-0453, March 1982.

[16]Hsieh, T. and Coakley, T. J., "Unsteady Separated Boundary Layer in a Transonic Diffuser Flow with Self-Excited Oscillations," AIAA Paper 86-1037.

[17]Hsieh, T., "Downstream Boundary Effects on the Frequency of Self-Excited Oscillations in Transonic Diffuser Flow," AIAA Paper 87-0161, Jan. 1987.

[18]Hsieh, T., Bogar, T. J., and Coakley, T. J., "Numerical Simulation and Comparison with Experiment for Self-Excited Oscillations in a Diffuser Flow," AIAA Paper 85-1475, July 1985.